

Energy Sources, Part A: Recovery, Utilization, and Environmental Effects

ISSN: 1556-7036 (Print) 1556-7230 (Online) Journal homepage: www.tandfonline.com/journals/ueso20

Numerical study of the flow and heat transfer characteristics of microencapsulated phase change slurry

Enpei Wang & Lei Li

To cite this article: Enpei Wang & Lei Li (2023) Numerical study of the flow and heat transfer characteristics of microencapsulated phase change slurry, Energy Sources, Part A: Recovery, Utilization, and Environmental Effects, 45:4, 11925-11942, DOI: 10.1080/15567036.2023.2263401

To link to this article: https://doi.org/10.1080/15567036.2023.2263401

Published online: 12 Oct 2023.

Submit your article to this journal

Article views: 257

View related articles

View Crossmark data

Citing articles: 2 View citing articles

Full Terms & Conditions of access and use can be found at
https://www.tandfonline.com/action/journalInformation?journalCode=ueso20

ENERGY SOURCES, PART A: RECOVERY, UTILIZATION, AND ENVIRONMENTAL EFFECTS
2023, VOL. 45, NO. 4, 11925–11942
https://doi.org/10.1080/15567036.2023.2263401

Taylor & Francis
Taylor & Francis Group

Check for updates

Numerical study of the flow and heat transfer characteristics of microencapsulated phase change slurry

Enpei Wang and Lei Li

Fundamental Science on Nuclear Safety and Simulation Technology Laboratory, Harbin Engineering University, Harbin, China

ABSTRACT

Microencapsulated phase change material (MPC) slurry is created by combining phase change material with a carrier fluid that has superior heat transfer properties compared to ordinary water. MPC slurry is conventionally investigated as heat storage and working fluid in a variety of applications to reduce power consumption. This study numerically investigates the impact of several critical parameters on the heat transfer coefficient (HTC) of MPC slurry in a circular pipe, using Eulerian–Eulerian model. The right triangle curve, one of equivalent specific heat model (ESHM), was applied to evaluate the influence of different critical variable values specified as $T_{in} = 305$ K, $q_{wall} = -125 \sim -200$ kW/m^2, $a_v = 0 \sim 15\%$, $Re = 6290 \sim 13838$, and $D = 10 \sim 25$ mm. The results show that increasing the velocity develops local HTC and reduce the rate of heat transformation. Phase change processing takes roughly twice as long at 1.1 m/s as at 0.5 m/s. Additionally, the results demonstrate that a high concentration of MPC slurry is advantageous for energy storage, as the temperature of MPC slurry is maintained over a considerable distance in cooling conditions. At a velocity of 0.8 m/s, the outlet bulk temperature of MPC slurry at various concentrations is 2–6 K higher than that of water. Furthermore, the evaluation reveals that the HTC was largely determined by pipe size, which was the primary factor. The findings of this study are useful for optimizing energy systems that require thermal energy management.

ARTICLE HISTORY
Received 26 July 2023
Revised 30 August 2023
Accepted 22 September 2023

KEYWORDS
Microencapsulated phase change material; Eulerian–Eulerian model; flow characteristics; equivalent specific heat model; CFD

Introduction

The global energy consumption rise is a direct consequence of the expansion of both the world economy and the human population (Abdeali and Bahramian 2022). To address this issue, numerous solutions are presented, with one of the most important conceptions being thermal energy storage (TES), which possesses a great deal of potential for reducing the overall energy consumption for requests that require a constant power supply. Currently, there are three classical heat storage types for TES technologies: sensible, latent, and thermochemical (Ghasemi, Tasnim, and Mahmud 2022). Compared to the methods of sensible and thermomechanical heat storage, the approach of latent heat storage is more attractive. The phase change materials (PCMs) for latent heat storage are more chemically stable than thermochemical storage materials, have a higher heat capacity than sensible heat storage materials, and are relatively simple to employ (Cárdenas-Ramírez, Jaramillo, and Gómez 2020). Therefore, this approach of heat storage has garnered a significant amount of attention and has been extensively put into various purposes, including buildings (Khademi et al. 2022), solar energy (Yang et al. 2022), clothes (Prateepmaneerak et al. 2022), and so on.

The ice storage (IC) system is a common method of latent TES technologies because of high-fusion latent heat of the water (Afsharpanah et al. 2022). In recent years, IC system has been the subject of

CONTACT Lei Li lileiheu@hrbeu.edu.cn Fundamental Science on Nuclear Safety and Simulation Technology Laboratory, Harbin Engineering University, Harbin 150001, China

© 2023 Taylor & Francis Group, LLC

numerous investigations. A numerical investigation on the charging performance of an IC system made up of serpentine tubes and connecting plates was carried out by Afsharpanah et al. (2022). The results demonstrated that the charging rate of thick plates with complete coverage was increased by up to 18%. Zhang et al. (2023) experimentally and numerically studied the heat transfer performance of an innovative IC unit with a compact plate fin. They found that the compact fin structure of the IC unit improved heat transfer. More channels, smaller external space size, and lower fin spacing resulted in a higher solidification rate and storage capacity. Yan et al. (2023) assessed the performance enhancement of cold storage and cooling characteristics of IC systems. The average discharge rate was improved by 74.4% for employing the spiral fins, compared with the without spiral structure. In addition, developing other novel kinds of PCMs is getting a lot of attention in energy storage systems (Afsharpanah, Mousavi Ajarostaghi, and Arıcı 2022). Ma et al. (2023) fabricated a shape-stable PCM by incorporating polyethylene glycol into a dual-network hydrogel, integrated silver nanowires, and Ti3C2Tx MXenes. The thermal conductivity was increased for the value of 0.64 W/m·K, and phase change enthalpy remarkably reached 124.8 J/g. Zhang et al. (2023) introduced an innovative form-stable cold energy storage PCM that incorporated ice as the phase change component and a polyether-based 3D network. It demonstrated exceptional form retention and thermal characteristics. This PCM exhibited a durable cold-insulation performance, exhibiting 1.85 times longer maintenance of cold temperature compared to ice. Zhang et al. (2023) proposed a novel approach that involves the integration of branch-structured fins and Al_2O_3 nanoparticles to improve the solidification process of PCM. In their research, the solidification behavior could be greatly improved by introducing nanoparticles and metal fins into the mix. They stated the reason was attributable to the combined effects of thermal conduction and natural convection.

To prevent PCM leakage due to phase change, reduce reactivity with the outside environment, and improve heat transfer, encapsulation is used. The stability and endurance of PCM can be increased through encapsulation, making it more resistant to degradation as time passes (Tripathi, Shukla, and Rathore 2023). On the basis of the dimension of the shell material, the encapsulation of the PCM can either be done through the process of macroencapsulation or through the process of microencapsulation. For the macroencapsulation method, the PCM is encapsulated in a shell material with larger dimension (capsule size above 5 mm) (Rathore and Shukla 2019). PCM macroencapsulation has the ability to reduce energy consumption in building systems because of its low cost. Microencapsulation is the process of enclosing PCM in a shell with a diameter of between 0.5 μm and 5000 μm (Konuklu et al. 2015). Microencapsulation of PCMs offers numerous benefits over macroencapsulation, including increased charging and discharging rates, improved thermal and chemical stability, and greater reliability (Alam et al. 2015). They can be used in many fields involving smart food packaging, electronic cooling, and alternative energy. The polymeric components that makeup PCM shell cause heat transfer properties to be restricted, and hydrodynamic and thermodynamic parameters are noticeably distinguishable from the base pure water liquid due to the polymeric nature of the microencapsulated PCM (MPC) slurry shell components (Zhang et al. 2020). Many studies focused on the analysis of core and shell materials responsible for the efficient transformation of the latent heat in MPC (Dou et al. 2022). For instance, polymer materials are highly compact with great dispersion characteristics. These advantages have made polymer extracts such as polyurea, polystyrene, methyl methacrylate, and so on, to be highly sorted as the choice material for PCM shells (Zhao et al. 2022). Similarly, the mixed materials for the core are more prominent under different applications and phase change temperatures.

A new kind of working substance known as MPC slurry is created by dispersing the MPC into a single-phase fluid, with improved heat transmission capability. Moreover, numerous investigations have concentrated on thermo-fluid capabilities to improve its use. Several experiment and simulation studies provide a more nuanced perception of the physical stability, heat transfer coefficient (HTC), and local behavior of microencapsulation over a range of mass fluxes, slurry concentrations, and particle sizes. Also, different types of tubes used for MPC slurry have become a research topic to study flow and heat transfer (Chinnasamy et al. 2023). Currently, the preparation of MPC slurry, flow

resistance, and flow characteristics have all been experimentally investigated. For instance, a new MPC slurry was prepared by paraffin melamine resin MPC and base fluid for absolute ethanol and deionized water in Xu et al.'s (2022) work, which increased the viscosity and friction factor. Besides, the MPC slurry with a mass fraction of 10% has been found to have the maximum cooling efficiency, and the efficiency factor was 57.0% greater than that of the base fluid, due to its flow resistance and heat transmission characteristics. Mustapha et al. (2022) tried to eliminate the effects of the subcooling phenomena in several ways, including expanding the size of the PCM, using nucleating agents. The findings suggest that there was subcooling reduction as a result of an increase in the size of the microcapsule, and the same result was achieved from the experiment in which copper nanoparticles were embedded into PCM shells. Using a blend of nanoparticles and PCM particles, Mo et al. (2022) created hybrid slurries to take advantage of the properties of the constituent materials. The cooling performance was improved as compared to single slurries of MPC or nanoparticles because hybrid slurries have higher dispersion stability and thermal conductivity.

Many scientists have conducted numerical investigations of MPC slurry based on some simplified models. The single-phase model handling MPC slurry as if it were a single-phase fluid was utilized in several numerical studies to deal with the slurry. The primary factor is the treatment for the MPC slurry phase transition procedure that differentiates these models from one another, for example, the model of effective specific heat (Dai, Zhu, and Liu 2022), enthalpy (Zeng et al. 2009), and so on. The single-phase model produced satisfactory results. However, there are noticeable weaknesses. The single-phase approach could not be used to adequately study the interactions between the capsules, as well as between the capsule and tube wall. The mixture model, as the homogeneous method for the multiphase flow model, could address this problem by solving continuity, momentum, and energy equations for the mixture (Dai et al. 2021; Liu, Zhu, and Fang 2018). The Eulerian–Eulerian model had been proposed for researching the flow and heat transfer of MPC slurry to obtain a comprehensive understanding of the two-phase flow. In this model, the governing equations were separately solved for each phase, allowing for a more comprehensive analysis of two-phase flow. It was proved greatly for anticipating the variations in the solid particle concentrate, and the energy transport performance can be estimated precisely (Ms and Venkatasubbaiah 2021). Therefore, this model is advantageous to simulate the flow and heat transfer performance of MPC slurry (M S and Venkatasubbaiah 2022).

As one of the effective specific heat methods (ESHMs), the rectangular curve was frequently used to anticipate the phase transition process inside the capsule for two-phase models in the literature (Dai and Liu 2023). However, different specific heat functions should be considered to select the optimal curve in numerical simulation. Additionally, very few numerical studies have examined the flow and heat transfer characteristics of MPC slurry under cooling conditions. Examining the heat transfer performance of MPC slurry with an appropriate specific heat curve is crucial in cooling. Consequently, this study proposes the two-phase Eulerian–Eulerian model application to numerically study flow and HTC of MPC slurries during cooling conditions under constant wall heat flux. This numerical method is effectively validated by available experiment data including temperature and pressure drop. Moreover, five different simplified curves of the ESHM are analyzed to search the optimal fit. The flow and heat transfer performance are evaluated with various parameters. The contour of temperature is also employed to visibly study the phase change process in the pipe. The result presented in this work is applicable for studying MPC slurry performance in cooling conditions, common in the heating ventilation and air conditioning system, TES, building environment, and other applications that require TES management as seen in previous studies.

Background: physical model and mathematical analysis

Working condition description

This paper gives a numerical analysis of a 2.0-m-long and 15-mm-diameter 3D geometrical model. To solve this model numerically, several assumptions are considered as follows:

(1) The MPC is evenly dispersed throughout the carrying fluid (water). Based on the results of Qiu and Li's (2020) experimental data, the MPC slurry containing less than 25% volumetric concentrations can be regarded as a Newtonian fluid.
(2) Incompressible and steady-state flow condition is assumed. The turbulent flow Reynolds number range is Re = 6400~15350 (v = 0.5~1.1 m/s).
(3) The thermophysical properties are assumed to be constant, with the exception of specific heat, which is highly dependent on temperature.
(4) For the present simulations, n-octadecane is used as the PCM and melamine-formaldehyde as the polymer shell, as specified by Yamagishi et al. (1999). As a long-chain hydrocarbon, n-octadecane is a desirable PCM due to its excellent heat energy storage performance, non-toxicity, and thermal regulation in an appropriate phase-change temperature range (Zhang et al. 2013). It has a higher latent heat than other PCMs within the same phase change temperature range (Zhang, Wang, and Wu 2010). In the current simulation, a volume fraction of 0–20% of MPC slurry is used, and Table 1 shows the MPC slurry and its thermophysical properties.

Governing equations

The dispersed phase is viewed for continuous fluid in Eulerian–Eulerian two-fluid model for slurry flow, interpenetrating and interacting with the liquid phase. The mathematical model could be described as follows:
Continuity equation:

$$\frac{\partial}{\partial t}\left(\alpha_i \rho_i\right) + \quad \cdot \left(\alpha_i \rho_i\right) = 0 \tag{1}$$

The subscript, i= l or i = s, represents the liquid or solid phase of the mixture.
Momentum equation:

$$\frac{\partial}{\partial t}\left(\alpha_i \rho_i \overrightarrow{v_i}\right) + \quad \cdot \left(\alpha_i \rho_i \overrightarrow{v_i}\,\overrightarrow{v_i}\right) = -\alpha_i \quad P + \quad \cdot \tau_i + \alpha_i \rho_i \vec{g} + K_{sl}\left(\overrightarrow{v_s} - \overrightarrow{v_l}\right) + \vec{F}_{lift,i} + \vec{F}_{vm,i} + \vec{F}_{td,i} \tag{2}$$

where P is the pressure and ($\vec{F}_{lift,i}$, $\vec{F}_{vm,i}$, $\vec{F}_{td,i}$) represents interfacial forces, lift force, and turbulent dispersion force, respectively, which are the interphase forces that dominate the turbulent flow.

The phase for liquid and solid phase stress–strain tensors can be determined separately as:

$$\tau_l = \alpha_l \mu_l \left[\quad \overrightarrow{v_l} + \left(\quad \overrightarrow{v_l}\right)^T\right] - \frac{2}{3}\alpha_l \mu_l \quad \cdot \overrightarrow{v_l} I \tag{3}$$

$$\tau s = \alpha_s \mu_s \left[\quad \overrightarrow{v}_s + \left(\quad \overrightarrow{v_s}\right)^T\right] + \alpha_s\left(\lambda_s - 23\mu_s\right) \quad \cdot \overrightarrow{v_s} I \tag{4}$$

Table 1. The thermophysical properties of MPC slurry (Yamagishi et al. 1999).

Materials	ρ/(kg/m^3)	c_p/(KJ/kg K)	k/(W/m K)	ΔH/(kJ/kg)	μ/(N/m^{2}s)
Core (solid)	850	1.800	0.340	223	-
Core (liquid)	780	2.200	0.150	-	-
Polymer shell	1,490	1.670	0.420	-	-
Water	997	4.180	0.610	-	0.87
MPC particle (solid)	1,000	1.754	0.310	167	-
MPC particle (liquid)	936	2.014	0.144	-	-
MPC slurry (7 vol%)	998	4.009	0.597	10.2	1.17
MPC slurry (12 vol%)	998	3.887	0.571	17.4	1.19
MPC slurry (20 vol%)	998	3.694	0.546	29.1	3.71

The solid's bulk viscosity, λ_s, can be expressed by Kumar, Gopaliya, and Kaushal (2019) and is modeled as:

$$\lambda_s = \frac{4}{3}\alpha_s d_p \rho_s g_o (1+e_p)\left(\frac{\Theta}{\pi}\right)^{1/2} \tag{5}$$

where g_o is the radial distribution function provided by Zhang et al. (2022):

$$g_o = \frac{1}{1-(\alpha_s/\alpha_{s,\max})^{1/3}} \tag{6}$$

The expression for shear viscosity of solid μ_s is given:

$$\mu_s = \mu_{s,\mathrm{col}} + \mu_{s,\mathrm{kin}} + \mu_{s,\mathrm{fr}} \tag{7}$$

where

$$\mu_{s,col} = \frac{4}{5}\alpha_s \rho_s d_s g_o (1+e_{ss})\left(\frac{\Theta_s}{\pi}\right)^{1/2} \tag{8}$$

$$\mu_{s,\mathrm{kin}} = \frac{\alpha_s d_s \rho_s \sqrt{\Theta_s \pi}}{6(3-e_{ss})}\left[1+\frac{2}{5}(1+e_{ss})(3e_{ss}-1)\alpha_s g_o\right] \tag{9}$$

$$\mu_{s,fr} = \frac{P_s \sin\varphi}{2\sqrt{I_{2D}}} \tag{10}$$

Energy equation:

$$\partial\partial t(\alpha_i \rho_i H_i) + \quad \cdot(\alpha_i \rho_i \overrightarrow{v_i} H_i) = \quad \cdot(k_b \quad T) + \overline{\overline{\tau}}_i : \quad \overrightarrow{v_i} - h_{sl} A (T_i - T_q) \tag{11}$$

where H means enthalpy tensor, $\overline{\overline{\tau}}_i$ is a stress–strain tensor, and k_b denotes effective bulk thermal conductivity.

The term h_{sl} is expressed as:

$$h_{sl} = \frac{k_l}{d_p} Nu_p \tag{12}$$

The value of Nu_p proposed by Gunn (Gunn 1978) and its expression is formulated as:

$$Nu_p = \left(7-10\alpha_l+5\alpha_l^2\right)\left(1+0.7Re_s^{0.2}P^{1/3}\right) + \left(1.33-2.4\alpha_l+1.2\alpha_l^2\right)\mathrm{Re}_s^{0.7}Pr^{\frac{1}{3}} \tag{13}$$

Based on the particle model, the parameter interfacial concentration A is introduced and can be expressed as:

$$A = \alpha_s A_s = \frac{6\alpha_s}{d_s} \tag{14}$$

Drag force model

The term K_{sl} is the drag force momentum exchange coefficient, which applies to all ranges of volume fraction.

$$K_{sl} = \begin{cases} \frac{3}{4} C_d \frac{\alpha_l \alpha_s \rho_l \left| \overrightarrow{v_l} - \overrightarrow{v_s} \right|}{d} \alpha_l^{-2.65} (\alpha_l > 0.8) \\ 150 \frac{\alpha_s^2 \mu_l}{\alpha_l d^2} + 1.75 \frac{\alpha_s \rho_l \left| \overrightarrow{v_l} - \overrightarrow{v_s} \right|}{d} (\alpha_l \leq 0.8) \end{cases} \tag{15}$$

where C_d is the drag coefficient:

$$C_d = \begin{cases} \frac{24}{Re_p} \left(1 + 0.15 Re_p^{0.687}\right) Re_p \leq 1000 \\ 0.44 Re_p > 1000 \end{cases} \tag{16}$$

where Re_p is the particle Reynolds number and modeled by:

$$Re_p = \frac{\rho_l d_s |-|}{\mu_l} \tag{17}$$

Thermophysical properties of MPC slurry

The MPC slurry consists of MPC particles and carrier fluid (water). The thermal conductivity of the MPC particle is calculated by Ran et al. (2022) as:

$$\frac{1}{k_p \cdot d_p} = \frac{1}{k_c \cdot d_c} + \frac{d_p - d_c}{k_s \cdot d_p \cdot d_c} \tag{18}$$

The bulk thermal conductivity is evaluated by Wang and Lin (2012), as:

$$k_b = \left[\frac{2k_w + k_p + 2\alpha_v (k_p - k_w)}{2k_w + k_p - \alpha_v (k_p - k_w)} \right] k_w \tag{19}$$

The characteristics of the MPC particles have an impact on the slurry's viscosity. The Vand equation was commonly used for calculating viscosity and expressed as follows:

$$\mu_b = \frac{\mu_w}{\left(1 - \alpha_v - B\alpha_v^2\right)^{2.5}} \tag{20}$$

where B is constant depending on the diameter and volume fraction of the particle and taken as 3.7 from the experiment of Yamagishi et al. (1999).

The specific heat capacity and density of the MPC slurry are expressed as:

$$c_b = \alpha_m c_{p,MPC} + (1 - \alpha_m) c_{p,w} \tag{21}$$

$$\rho_b = (1 - \alpha_v) \rho_w + \alpha_v \rho_{MPC} \tag{22}$$

where α_m and α_v are a fraction of mass and volume, respectively.

The specific heat of MPC can be simplified by the ESHM method during simulation in freezing conditions (Zhang et al. 2003). Four different equivalent specific heat functions have been taken into consideration, which are analyzed in detail in the next section.

The coefficient of local convection heat transfer is determined by:

$$h = \frac{q_{wall}}{T_{wall} - T_b} \tag{23}$$

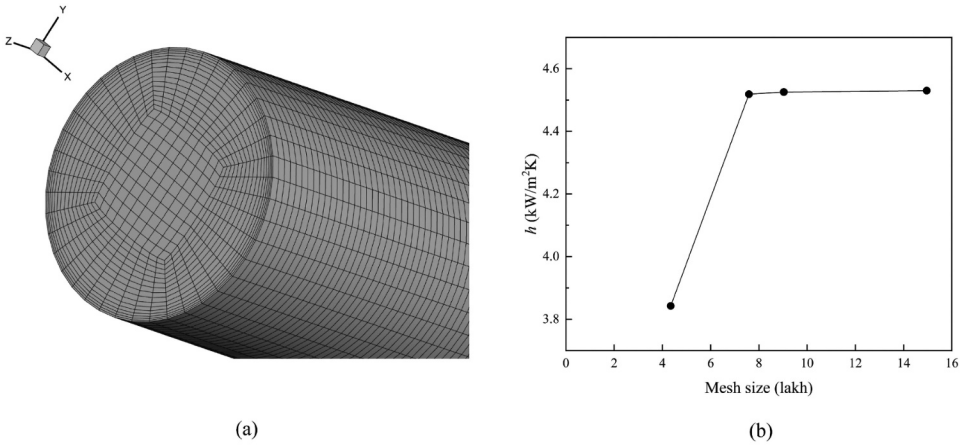

Figure 1. The mesh grid of pipe schematic.

Numerical description and validation

Boundary conditions

In this work, a circular pipe with a 2 m length and 15 mm diameter was developed. The ratio of length and the diameter of the pipe exceed 100 to guarantee that the outcomes of fully developed flow can be attained in each of instances. The two phases used the pressure outlet as the outlet boundary and a constant velocity as the input. The MPC slurry is heated continuously by heat flux applied for the wall boundary condition. In the flow, the particle was evenly distributed with a 6.3 μm diameter.

Numerical method

A two-phase Eulerian–Eulerian model is solved by ANSYS Fluent code (v17, Ansys, Canonsburg, PA, USA), based on the finite volume analysis method in present simulation. The pressure-based and steady state solver are set in numerical operation. Pressure velocity coupling is solved by the SIMPLE algorithm, and the energy and momentum equations are solved by the Second Order Upwind. The convergence criterion for the governing equations consisting of the continuity equation, momentum, and energy equations is set at 10^{-6}. The heat transfer fluid adopted the RNG k-epsilon model, which

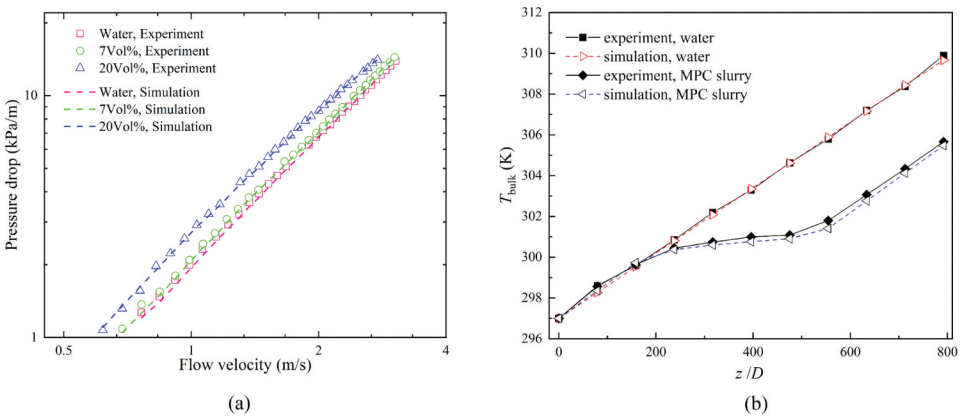

Figure 2. Comparisons between CFD results and experimental data. (a) Pressure drop and (b) temperature.

Table 2. The range of parameters in numerical simulation.

Parameters	Unit	Range
q_{wall}	kW/m^2	−125~−200
α_v	-	0~15%
Re	-	6290~13838
D	mm	10~25

describes the turbulence transfer between different phases. The dispersed phases and their distributed mixture variants of the k-epsilon turbulence model are commonly employed in multiphase flow, due to their reasonable accuracy and inexpensive computing cost (Silva et al. 2015). The k-epsilon turbulence model for each phase is applied to describe the turbulence transfer between the two phases in the numerical simulation discussed in this work (Jiang and Zhang 2012).

Mesh independency and model validation

The geometrical model and the hexahedral structured mesh have been developed using ICEM software. The grid type and size in computational domain are shown in Figure 1a. Four different meshes are adapted for independent analysis of the outlet local convection HTC with 4.34, 7.59, 9.03, and 14.96 lakh. As depicted in Figure 1b, when the number of meshes increases from 7.59 lakh to 9.03 lakh, the deviation rate is 0.15%. When the number of meshes rises from 9.03 lakh to 14.96 lakh, the deviation rate is 0.10%. A grid size of 7.59 lakh is chosen for the subsequent investigation to assure model accuracy and rapid computation.

A numerical validation is done to confirm the reliability of this model, by comparing results presented by Yamagishi et al. (1999). The obtained results of pressure drop from numerical simulation using the Eulerian–Eulerian method in terms of various velocity is validated with experiment at the condition of temperature 298 K and heating load 0 kW. As depicted in Figure 2a, the comparisons show a good agreement with the maximum errors are 5.20%, 7.93%, and 4.22% for water, 7 vol%, and 12 vol% MPC slurry separately. The pressure drop increases with concentration development, where the viscosity poses a significant role. The MPC slurry of α_v = 0.12 and carried fluid flow velocity of 1.25 m/s with an inner diameter, D, of 10.1 mm, and length z of 8 m under 5 kW constant wall heat flux are the same experimental conditions and geometry structure. Figure 2b shows the comparison of the local bulk mean temperature in nondimensional length for both fluids between the experiment and Computaional Fluid Dynamics (CFD) work. A three-stage tread of the bulk mean temperature in the axial position for MPC slurry is completely dissimilar in contrast with the pure water flowing increasing linearly. The temperature ascents rapidly at the entrance and outflow flowing test section, while it stays relatively constant between 300 and 500 of nondimensional length. The reason for the flat region appearance is the existence of latent heat that absorbed or released a significant quantity of TES. Besides, the developing rate for bulk mean temperature was not sufficiently compared with experimental data. It may result from the influence of the secondary flow that enhanced the MPC slurry bulk temperature (Liu, Zhu, and Fang 2018). From this, it is possible to deduce that the numerical model shape is feasible in analyzing the flow properties and HTC of MPC slurry from the high degree of congruence between numerical and experimental distinction. The range of parameters in the present study is presented in Table 2.

Results and discussion

To research the flowing characteristics and HTC of MPC slurry in freezing conditions, this work computationally simulated and analyzed pure water and MPC slurry in a volume concentration range between 7% and 15%. The combination is subjected to tests under similar operating conditions. In the first step of this process, the four primary equivalent curves of the ESHM method for MPC slurry were

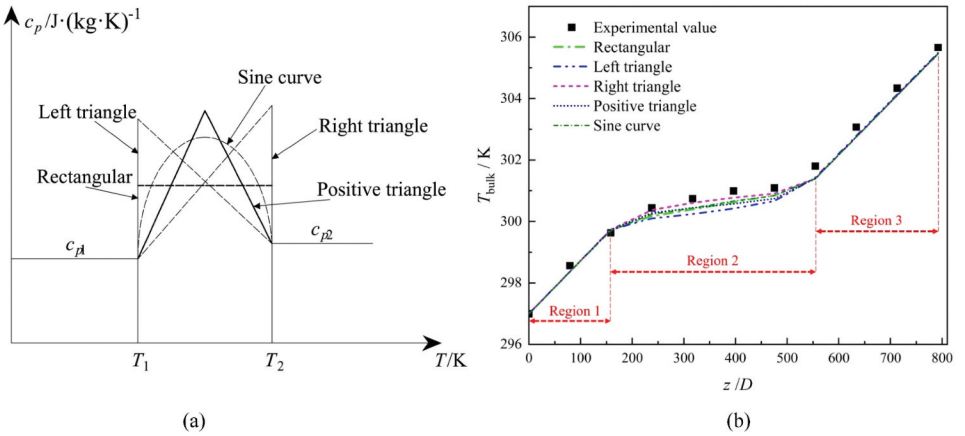

Figure 3. Different simplification methods (a), comparing with experiment (b).

studied for numerical simulation in comparison with the experimental result. After that, the simplification approach with the smaller error was adopted for further analysis. Performance assessment and parameter analysis were executed to numerically analyze operating characteristics and HTC for MPC slurry, such as the input velocity and the wall heating flux.

The influence of the processing method on the ESHM

The phase transition process does not practically occur at a certain temperature point rather throughout a broad temperature gradient when it is modeled for numerical simulations of the MPC. As a result, this issue is remedied using the ESHM approach in a simpler manner presented by Hu and Zhang's (2002) study. This approach treats the specific heat capacity the same as a temperature single-valued function, which is normally handled in triangular, sine, or rectangular shapes. Nevertheless, the surrounding area remains the same, as illustrated in Figure 3a. The area between T_1 and T_2 represents the sum of the latent and sensible heat of the MPC as shown in Figure 3a and the equation could be described as follows:

$$\int_{T_1}^{T_2} c_p dT = LH + c_{p,avg}\Delta T \tag{24}$$

where LH and ΔT are latent heat of the MPC and phase change temperature range, respectively. $c_{p,avg}$ is the average specific heat of c_{p1} and c_{p2}.

In some analyses, c_{p1} and c_{p2} are simplified to the point where they are completely identical to one another so that the calculation may be performed with greater ease (Zhang, Hu, and Wang 2003). However, when it comes to the actual working circumstances, there are a few key considerations that need to be addressed about the setting of the specific heat capacity. Therefore, the effective specific heat capacity for each of the cases at the temperature phase change region was deduced in this work and described as follows (Alisetti and Roy 2000; Zhang and Qian 2013):

(1) Rectangular

$$c_p = \frac{1}{2}\left(c_{p1} + c_{p2}\right) + \frac{LH}{T} \tag{25}$$

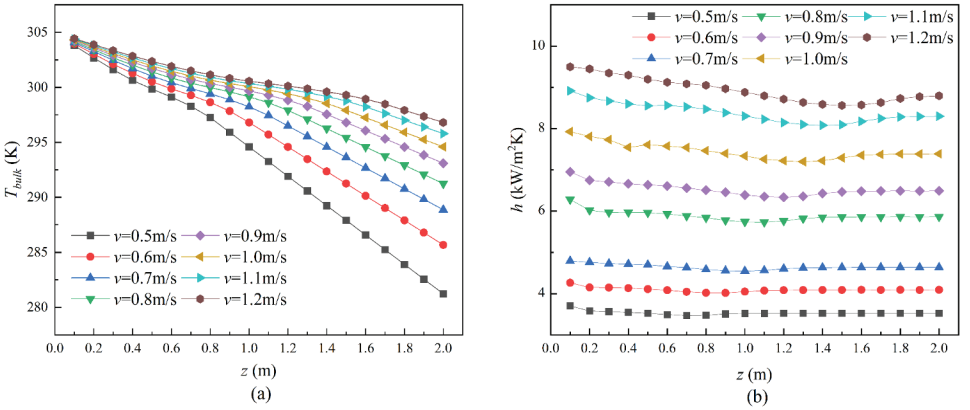

Figure 4. The effect of different inlet velocities. (a) Temperature and (b) local HTC.

(2) Left triangle

$$c_p = c_{p1} + (c_{p2} - c_{p1}) \cdot (T - T_1)\Delta T + 2LH \cdot (T_2 - T)(\Delta T)^2 \tag{26}$$

(3) Right triangle

$$c_p = c_{p_1} + \frac{(c_{p_2} - c_{p_1}) \cdot (T - T_1)}{\Delta\ T_1} + \frac{2LH \cdot (T - T_1)}{(\Delta\ T)^2} \tag{27}$$

(4) Positive triangle

$$c_p = \begin{cases} c_{p_1} + \left[\frac{c_{p_2} - c_{p_1}}{\Delta\ T} + \frac{4LH}{(\Delta\ T)^2}\right](T - T_1) T_1 < T \leq \frac{T_1 + T_2}{2} \\ c_{p_2} + \left[\frac{4LH}{(\Delta\ T)^2} - \frac{c_{p_2} - c_{p_1}}{\Delta\ T}\right](T_2 - T) \frac{T_1 + T_2}{2} < T < T_2 \end{cases} \tag{28}$$

(5) Sine curve

In the scenario discussed in this work, the sine curve is notoriously difficult to acquire an analytical solution and instead requires the use of numerical solutions in the scenario presented to be generated. To simplify the analysis, the sine curve is solved as follows:

$$c_p = c_{p,avg} + \left[\frac{\pi}{2} \cdot \left(\frac{LH}{\Delta T} - c_{p,avg}\right) \cdot \sin(\pi \cdot \frac{T - T_1}{\Delta T})\right] \tag{29}$$

Different equivalent specific heat models are adopted and compared with the result from Yamagishi et al. (1999) in Figure 3b. There is hardly any difference between Region 1 and Region 3. The right triangle curve is the most accurate when compared with the experimental data in Region 2. The three curves have very little difference under the parameters of the rectangle, sine, and positive triangle, but the left triangle has the most noticeable variation with the experimental data. Therefore, the right triangle curve is fitted in the latter numerical simulation. Simultaneously, the temperature range of Region 2 is considered as the phase change process between the temperature of 299.6 to 301.8 K in the present study.

Influence of velocity on heat transfer of MPC slurry

The current simulation utilized the following parameters: $\alpha_v = 0.07$, $q_{wall} = -100\ \mathrm{kW/m^2}$, and $T_{\mathrm{in}} = 305$ K to examine the effective inlet velocity on the local convective HTC of MPC slurry the over velocity ranges from 0.5 m/s to 1.1 m/s with Re range of 6,400 to 15,350. As shown in Figure 4a, the

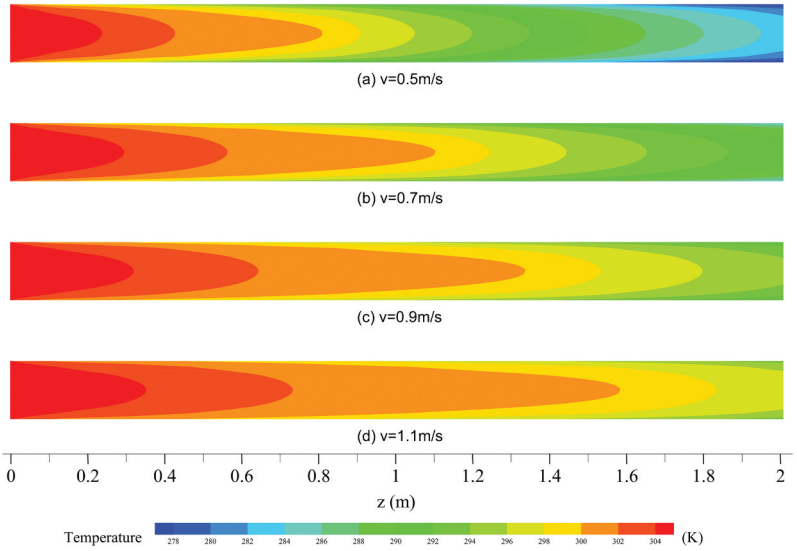

Figure 5. Temperature distribution of MPC slurry under different velocities.

temperature decreases slowly with inlet velocity increasing along pipe axis distance. Besides, the local bulk temperature is closer to the phase change range at high velocity. Figure 4b displays the variations of local HTC along the MPC slurry flow direction at different velocity ranges. It has been witnessed that local HTC declined gradually until it reached its lowest, after which it progressively rose until it reached a flat state at the end of the pipe for high inlet velocity curves, while it has no obvious trends for lower velocity. The reason for this is that the amount of solidifying MPC grows along the flow direction, which means that an increased flow distance results in an increased amount of energy being absorbed as sensible heat. In addition, the MPC slurry with the lower flow rate achieved the phase transition temperature sooner, and as the MPC continued solidifying, there was only a tiny difference in temperature along the flow direction. Therefore, the reason that the variation of temperature unsimultaneously exists for the wall and fluid resulted in the local convective HTC remaining almost the same. The local HTC is enhanced to some extent by increased turbulence caused by the variation in viscosity of the MPC slurry as a function of temperature when the percentage of MPC cools continues to grow.

At the region of flowing fully developed, the local HTC remains unaltered scarcely to some degree. The temperature field of MPC slurry along the flowing section with velocity difference is shown in Figure 5. As can be observed, raising the velocities results in an improved bulk temperature. Additionally, the HTC is enhanced in regions with higher velocities where the phase transition zone was enlarged. The length of phase change processing at a velocity of 1.1 m/s is almost two times higher than the velocity of 0.5 m/s. As a result, the HTC at a given location was generally proportional to the velocity of the incoming flow.

Influence of concentration on heat transfer of MPC slurry

Another major aspect that has a major impact on determining the local HTC of an MPC slurry is the concentration of the slurry, which refers to the volume fraction of microcapsules that are present in the slurry. To study the impact on heat transfer of the MPC slurry, several concentrations ranging from 0% to 20% were selected in the numerical simulations under the following conditions: $T_{\text{in}} = 305\text{K}$, $q_{\text{wall}} = -150\ \text{kW/m}^2$, $v = 0.8\ \text{m/s}$. The temperature of water decreases linearly along axis distance, while the MPC slurry in different concentrations change in low velocity rate at phase change range as

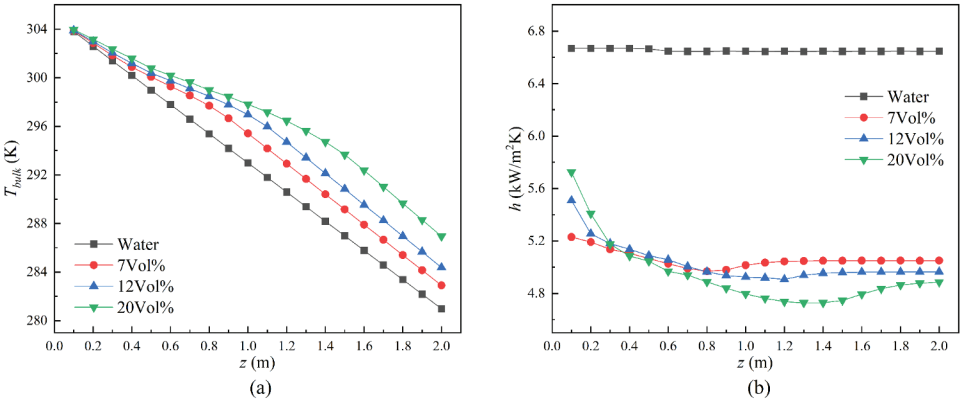

Figure 6. The effect of various concentrations. (a) Temperature and (b) local HTC.

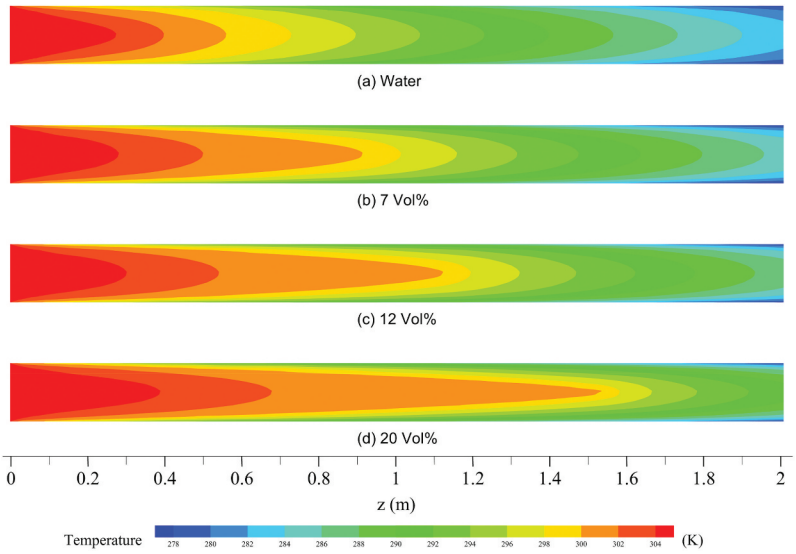

Figure 7. Distribution of temperature under different concentrations.

shown in Figure 6a. After phase changing, the temperature of MPC slurry keeps the same declining trend with water. As shown in Figure 6b, the local HTC varies hardly for the water, while it maintains a low value to the MPC slurry because of the presence of PCM. It is essential to consider the fact that MPC phase transition may prevent the average bulk temperature from shifting. The MPC phase change period lasts longer for the high-concentration slurry and the MPC freezes later than the low-concentration slurry at the outlet, which is demonstrated in Figure 7. As the single-phase fluid, the temperature of water remains an equidistance distribution under constant heat flux. The MPC in slurry improved with the increase in initial concentration enhancing the bulk temperature in cooling. Therefore, the MPC slurry in high concentration is important to maintain the temperature during the cooling range and advantageous for energy storage.

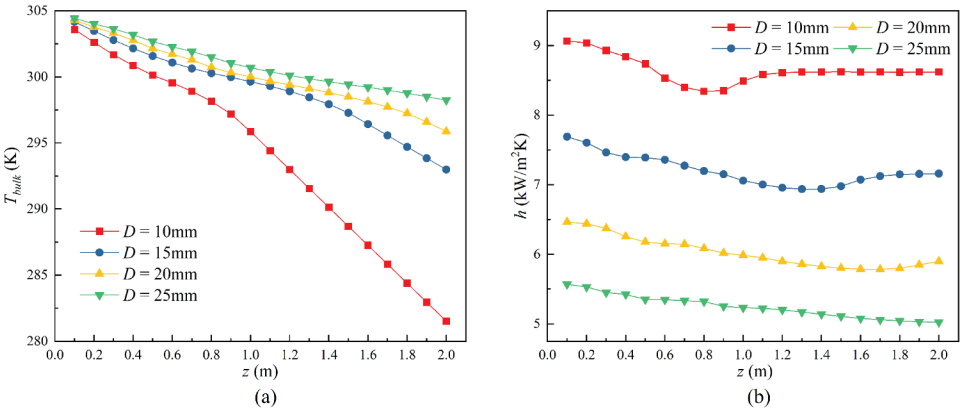

Figure 8. The effect of different pipe diameters. (a) Temperature and (b) local HTC.

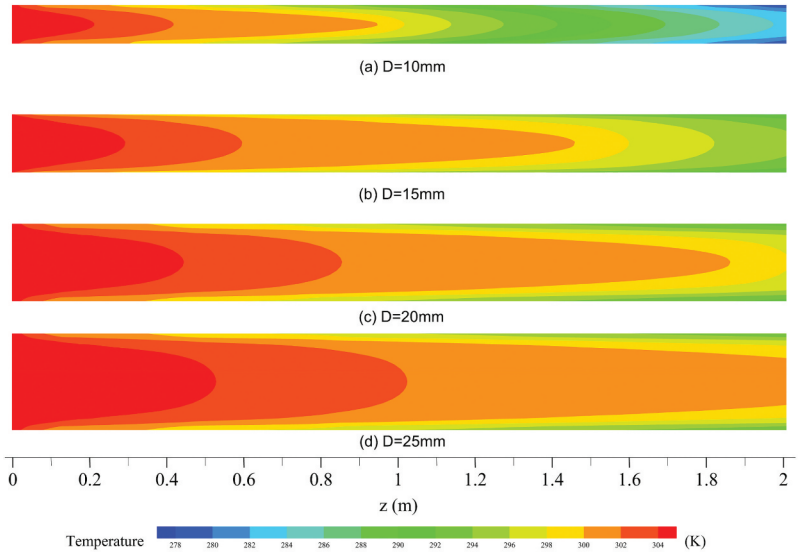

Figure 9. Distribution of temperature under various pipe diameters.

Influence of diameter on heat transfer of MPC slurry

There are various pipe standards available, making pipe size a crucial variable to study. For the pipe of considerable size, the performance of heat transmission is affected critically by radical long distance. However, a pipe of miniature size also poses a negative impact on heat transmission because of the large pipe–particle ratio. Therefore, it is important to evaluate the heat transfer with different pipe sizes in cooling. The bulk temperature is increasing in larger pipe diameters and is close to the temperature range of phase change, as shown in Figure 8a. Figure 8b depicts the local convective HTC along the pipe for a range of pipe diameters under the condition of $T_{\text{in}} = 305\text{K}$, $q_{\text{wall}} = -125\ \text{kW/m}^2$, $v = 1.0\ \text{m/s}$, and $\alpha_v = 0.12$. The local HTC has a little change along the pipe flow direction, while it is significantly affected by the pipe diameter. It is about two times as much for a pipe with a diameter of 10 mm as compared to one with a diameter of 25 mm. The difference in temperature between the pipe wall and the mean temperature of the fluid was less, which led to a higher HTC. The pipe in tiny size will

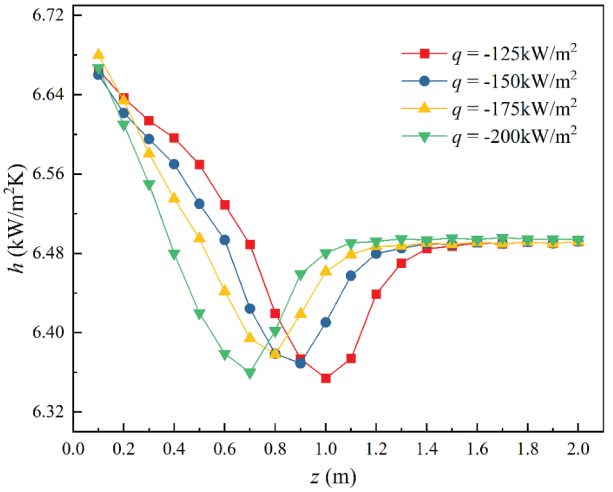

Figure 10. HTC of the MPC slurry under different heating fluxes.

beneficially facilitate the heat transfer adequately as the HTC definition. Therefore, it can be deduced that the HTC was largely determined by the pipe size, which was the primary factor at play. Meanwhile, the phase change area develops with increasing pipe size, which can be observed in Figure 9.

Influence of wall heat flux on local HTC of MPC slurry

Local HTCs with several wall heat fluxes in the axial direction are shown in Figure 10 under the following conditions: Tin = 305K, $\alpha_v = 0.07$, and v = 0.9 m/s. The local HTC declines rapidly to nadir and then increases for all curves along the axis distance. The trend can be accelerated at lower heat flux because the phase change process is improved. After the process, the local HTC has maintained an almost constant value for various heat fluxes. This reason for the flat curve can be related to the thermophysical properties, which are in negligible variations and pose a slight impact on the heat transfer of MPC slurry in a pipe. Therefore, the wall heat flux can enhance the phase change process of MPC slurry, while it brings less influence on the local HTC.

Conclusions

A numerical investigation of heat transfer and flow characteristics based on two-phase Eulerian–Eulerian models in freezing conditions was analyzed in the present study. The influence of Reynolds number, concentration and pipe diameter, and wall heat flux in the flowing direction were studied and evaluated. The key conclusions of the study are summarized below:

(1) The approach of ESHM presented significantly simplified the analysis of the specific heat capacity of a freezing MPC slurry. The right triangle curve was fitted remarkably with experimental data among the five curves of the ESHM method and employed in the following simulation.
(2) Increase in velocity improves the HTC and the phase change area of the MPC slurry. The temperature drops slowly with inlet velocity increasing in cooling conditions. Phase change processing takes roughly twice as long at 1.1 m/s as at 0.5 m/s. The local HTC is proportional to the flow inlet velocity.

(3) The bulk temperature decreases linearly, and the local HTC stays in constant condition for the water along the flow direction compared with the MPC slurry. The local HTC for MPC slurry in various concentrations is lower than water because of phase change. The MPC phase change lasts longer for high-concentration slurry, which raises the bulk temperature, and the MPC cools later than the low-concentration slurry at the outlet. At a velocity of 0.8 m/s, the outlet bulk temperature of MPC slurry at various concentrations is 2–6 K higher than that of water.
(4) The local HTC was largely influenced by the pipe size. That is, a smaller pipe size leads to more efficient heat exchange. The MPC slurry is still in the phase change range in large diameter pipe, which keeps the bulk temperature higher. Thus, the transportation of MPC slurry in large diameter is advantageous to maintain the temperature under cooling conditions.
(5) The phase change process can be improved at lower wall heat flux. However, it poses a negligible impression on the local HTC after phase changing along axis distance.

For the future work, the numerical simulation model for a deeper comprehension of the flow and heat transfer interactions requires additional research. Furthermore, the heat transfer analysis of MPC slurry with the addition of nanoparticles should be considered to improve heat transfer performance further.

Nomenclatures

A	interfacial area, m^2
c_p	specific heat capacity, KJ/kg K
D	diameter of the pipe, mm
h	heat transfer coefficient, kW/m^2 K
K	thermal conductivity, W/m K
LH	latent heat, J/kg
P	pressure, Pa
Q	heat flux, kW/m^2
Re	Reynolds number
T	temperature, K
v	velocity, m/s
Z	length along the pipe, m
Subscripts	
b	bulk MPC slurry
l	liquid phase
m	mass
p	MPC particle
s	solid phase
sl	phases interaction
w	carrier fluid (water)
Greek letters	
α	volume fraction
μ	viscosity, N/m^2 s
ρ	density, kg/m^3

Disclosure statement

No potential conflict of interest was reported by the author(s).

ORCID

Enpei Wang http://orcid.org/0000-0002-4160-3997

References

Abdeali, G., and A. R. Bahramian. 2022. A comprehensive review on rheological behavior of phase change materials fluids (slurry and emulsion): The way toward energy efficiency. *Journal of Energy Storage* 55:105549. doi:10.1016/j.est.2022.105549.

Afsharpanah, F., S. S. Mousavi Ajarostaghi, and M. Arıcı. 2022. Parametric study of phase change time reduction in a shell-and-tube ice storage system with anchor-type fin design, *International Communications in Heat and Mass Transfer* 137:106281. doi:10.1016/j.icheatmasstransfer.2022.106281.

Afsharpanah, F., K. Pakzad, S. S. Mousavi Ajarostaghi, and M. Arıcı. 2022. Assessment of the charging performance in a cold thermal energy storage container with two rows of serpentine tubes and extended surfaces, *Journal of Energy Storage* 51:104464. doi:10.1016/j.est.2022.104464.

Afsharpanah, F., K. Pakzad, S. S. Mousavi Ajarostaghi, S. Poncet, and K. Sedighi. 2022. Accelerating the charging process in a shell and dual coil ice storage unit equipped with connecting plates. *International Journal of Energy Research* 46 (6):7460–78. doi:10.1002/er.7654.

Alam, T. E., J. S. Dhau, D. Y. Goswami, and E. Stefanakos. 2015. Macroencapsulation and characterization of phase change materials for latent heat thermal energy storage systems. *Applied Energy* 154:92–101. doi:10.1016/j.apenergy.2015.04.086.

Alisetti, E. L., and S. K. Roy. 2000. Forced convection heat transfer to phase change material slurries in circular ducts. *Journal of Thermophysics and Heat Transfer* 14 (1):115–18. doi:10.2514/2.6499.

Cárdenas-Ramírez, C., F. Jaramillo, and M. Gómez. 2020. Systematic review of encapsulation and shape-stabilization of phase change materials, *Journal Energy Storage* 30:101495, doi:10.1016/j.est.2020.101495.

Chinnasamy, V., J. Heo, S. Jung, H. Lee, and H. Cho. 2023. Shape stabilized phase change materials based on different support structures for thermal energy storage applications–A review. *Energy* 262:125463. doi:10.1016/j.energy.2022.125463.

Dai, H., W. Chen, Q. Cheng, Y. Liu, and X. Dong. 2021. Analysis of thermo-hydraulic characteristics in the porous-wall microchannel with microencapsulated phase change slurry. *International Journal of Heat and Mass Transfer* 165:120634. doi:10.1016/j.ijheatmasstransfer.2020.120634.

Dai, H., and Y. Liu. 2023. Entropy generation analysis on thermo-hydraulic characteristics of microencapsulated phase change slurry in wavy microchannel with porous fins. *Applied Thermal Engineering* 219:119440. doi:10.1016/j.applthermaleng.2022.119440.

Dai, H., C. Zhu, and Y. Liu. 2022. Thermal performance of double-layer porous-microchannel with phase change slurry. *Applied Thermal Engineering* 211:118457. doi:10.1016/j.applthermaleng.2022.118457.

Dou, G., G. Peng, Y. Hu, Y. Sun, H. Jiang, and T. Zhang. 2022. Effects of interface bonding on the macro-mechanical properties of microcapsule/epoxy resin composites. *Surfaces Interfaces* 34:102310. doi:10.1016/j.surfin.2022.102310.

Ghasemi, K., S. Tasnim, and S. Mahmud. 2022. PCM, nano/microencapsulation and slurries: A review of fundamentals, categories, fabrication, numerical models and applications. *Sustainable Energy Technologies*. 52:102084. doi:10.1016/j.seta.2022.102084.

Gunn, D. J. 1978. Transfer of heat or mass to particles in fixed and fluidised beds. *International Journal of Heat and Mass Transfer* 21 (4):467–76. doi:10.1016/0017-9310(78)90080-7.

Hu, X., and Y. Zhang. 2002. Novel insight and numerical analysis of convective heat transfer enhancement with microencapsulated phase change material slurries: Laminar flow in a circular tube with constant heat flux. *International Journal of Heat and Mass Transfer* 45 (15):3163–72. doi:10.1016/S0017-9310(02)00034-0.

Jiang, Y. Y., and P. Zhang. 2012. Numerical investigation of slush nitrogen flow in a horizontal pipe. *Chemical Engineering Science* 73:169–80. doi:10.1016/j.ces.2012.01.027.

Khademi, A., K. Shank, S. A. A. Mehrjardi, S. Tiari, G. Sorrentino, Z. Said, A. J. Chamkha, and S. Ushak. 2022. A brief review on different hybrid methods of enhancement within latent heat storage systems, *Journal Energy Storage* 54:105362. doi:10.1016/j.est.2022.105362.

Konuklu, Y., M. Ostry, H. O. Paksoy, and P. Charvat. 2015. Review on using microencapsulated phase change materials (PCM) in building applications. *Energy Buildings* 106:134–55. doi:10.1016/j.enbuild.2015.07.019.

Kumar, N., M. K. Gopaliya, and D. R. Kaushal. 2019. Experimental investigations and CFD modeling for flow of highly concentrated iron ore slurry through horizontal pipeline. *Particulate Science Technology* 37 (2):232–50. doi:10.1080/02726351.2017.1364313.

Liu, L., C. Zhu, and G. Fang. 2018. Numerical evaluation on the flow and heat transfer characteristics of microencapsulated phase change slurry flowing in a circular tube. *Applied Thermal Engineering* 144:845–53. doi:10.1016/j.applthermaleng.2018.08.102.

M S, A., and K. Venkatasubbaiah. 2022. Numerical investigation on heat transfer performance of a confined slot jet impingement with different MEPCM-water slurries using two-phase Eulerian–Eulerian model. *Thermal Science and Engineering Progress* 33:101315. doi:10.1016/j.tsep.2022.101315.

Ma, Y., M. Zou, W. Chen, W. Luo, X. Hu, S. Xiao, L. Luo, X. Jiang, and Q. Li. 2023. A structured phase change material integrated by MXene/AgNWs modified dual-network and polyethylene glycol for energy storage and thermal management. *Applied Energy* 349:121658. doi:10.1016/j.apenergy.2023.121658.

Mo, S., J. Ye, L. Jia, andY. Chen. 2022. Properties and performance of hybrid suspensions of MPCM/nanoparticles for LED thermal management, *Energy* 239:122650. doi:10.1016/j.energy.2021.122650.

Ms, A., and K. Venkatasubbaiah. 2021. Numerical investigation on laminar forced convection of MEPCM-water slurry flow through a micro-channel using Eulerian-Eulerian two-phase model. *Thermal Science and Engineering Progress* 22:100803. doi:10.1016/j.tsep.2020.100803.

Mustapha, A., Y. Wang, Y. Ding, and Y. Li. 2022. Supercooling elimination of cryogenic-temperature microencapsulated phase change materials (MPCMs) and the rheological behaviors of their suspension. *Journal of Materials Research and Technology* 21:2277–95. doi:10.1016/j.jmrt.2022.10.010.

Prateepmaneerak, N., A. Chaiyasat, D. Kaewpa, and P. Chaiyasat. 2022. Innovative bifunctional heat storage nanocapsules containing polymerizable surfactant for antimicrobial thermoregulating clothes. *Colloids Surfaces A Physicochem Engineering Aspects* 653:129954. doi:10.1016/j.colsurfa.2022.129954.

Qiu, Z., and L. Li. 2020. Experimental and numerical investigation of laminar heat transfer of microencapsulated phase change material slurry (MPCMS) in a circular tube with constant heat flux. *Sustainable Cities and Society* 52:101786. doi:10.1016/j.scs.2019.101786.

Ran, F., H. Zhang, C. Xu, and G. Fang. 2022. Thermal performances evaluation of a flat-plate solar collector using microencapsulated phase-change slurry as heat transfer medium. *International Journal of Energy Research* 46 (10):14044–59. doi:10.1002/er.8121.

Rathore, P. K. S., and S. K. Shukla. 2019. Potential of macroencapsulated PCM for thermal energy storage in buildings: A comprehensive review. *Construction and Building Materials* 225:723–44. doi:10.1016/j.conbuildmat.2019.07.221.

Silva, R., F. A. P. Garcia, P. M. Faia, and M. G. Rasteiro. 2015. Evaluating the performance of the mixture model coupled with high and low Reynolds turbulence closures in the numerical description of concentrated solid-liquid flows of settling particles. *The Journal of Computational Multiphase Flows* 7 (4):241–57. doi:10.1260/1757-482X.7.4.241.

Tripathi, B. M., S. K. Shukla, and P. K. S. Rathore. 2023. A comprehensive review on solar to thermal energy conversion and storage using phase change materials, *Journal Energy Storage* 72:108280. doi:10.1016/j.est.2023.108280.

Wang, L., and G. Lin. 2012. Experimental study on the convective heat transfer behavior of microencapsulated phase change material suspensions in rectangular tube of small aspect ratio. *Bubbly Flows: Analysis, Modelling & Calculation* 48 (1):83–91. doi:10.1007/s00231-011-0844-2.

Xu, Q., L. Zhu, X. Yan, J. Yang, Z. Wang, D. Liu, G. Yang, X. Chen, N. Akkurt, L. Liu, Y. Du, Y. Qiang, and Y. Xiong. 2022. Heat transfer performance by forced convection of microencapsulated phase change material-latent functional thermal fluid flowing in a mini-channels heat sink. *Applied Thermal Engineering*. 216:119158. doi:10.1016/j.applthermaleng.2022.119158.

Yamagishi, Y., H. Takeuchi, A. T. Pyatenko, and N. Kayukawa. 1999. Characteristics of microencapsulated PCM slurry as a heat-transfer fluid. *AIChE Journal* 45 (4):696–707. doi:10.1002/aic.690450405.

Yan, W.-M., C.-Y. Huang, K.-E. Gao, M. Amani, L.-H. Chien, and A. Homayooni. 2023. Study on the performance enhancement of ice storage and melting processes in an ice-on-coil thermal energy storage system. *Journal of Energy Storage* 72:108410. doi:10.1016/j.est.2023.108410.

Yang, X., X. Wang, Z. Liu, X. Luo, and J. Yan. 2022. Effect of fin number on the melting phase change in a horizontal finned shell-and-tube thermal energy storage unit. *Solar Energy Materials and Solar Cells* 236:111527. doi:10.1016/j.solmat.2021.111527.

Zeng, R., X. Wang, B. Chen, Y. Zhang, J. Niu, X. Wang, and H. Di. 2009. Heat transfer characteristics of microencapsulated phase change material slurry in laminar flow under constant heat flux. *Appl Applied Energy* 86 (12):2661–70. doi:10.1016/j.apenergy.2009.04.025.

Zhang, B., S. Li, X. Fei, H. Zhao, and X. Lou. 2020. Enhanced mechanical properties and thermal conductivity of paraffin microcapsules shelled by hydrophobic-silicon carbide modified melamine-formaldehyde resin. *Colloids and Surfaces A: Physicochemical and Engineering Aspects*. 603:125219. doi:10.1016/j.colsurfa.2020.125219.

Zhang, C., W. Huang, C. Li, J. Ouyang, H. Wang, J. Xu, and H. Luo. 2022. Numerically investigating the effects of geometry on hydrodynamics and particle suspension performance in continuous oscillatory baffled crystallizers. *Chemical Engineering Science* 249:117352. doi:10.1016/j.ces.2021.117352.

Zhang, H., X. Wang, and D. Wu. 2010. Silica encapsulation of n-octadecane via sol–gel process: A novel microencapsulated phase-change material with enhanced thermal conductivity and performance. *Journal of Colloid and Interface Science* 343 (1):246–55. doi:10.1016/j.jcis.2009.11.036.

Zhang, J., Z. Cao, S. Huang, X. Huang, Y. Han, C. Wen, J. H. Walther, and Y. Yang. 2023. Solidification performance improvement of phase change materials for latent heat thermal energy storage using novel branch-structured fins and nanoparticles. *Applied Energy* 342:121158. doi:10.1016/j.apenergy.2023.121158.

Zhang, P., and W. Q. Qian. 2013. Investigation of laminar convective heat transfer of phase change material slurries in circular tubes. *Journal of Engineering Thermophysics* 34:1914–17. in Chinese.

Zhang, Y., M. He, G. Yuan, Y. Wang, T. Zhang, T. Wen, P. Gao, and Z. Wang. 2023. Effect of compact fin structure on heat transfer performance of ice storage unit during freezing. *Applied Thermal Engineering* 230:120775. doi:10.1016/j.applthermaleng.2023.120775.

Zhang, Y., X. Hu, Q. Hao, and X. Wang. 2003. Convective heat transfer enhancement of laminar flow of latent functionally thermal fluid in a circular tube with constant heat flux: Internal heat source model and its application. *Science in China Series E: Technological Sciences* 46 (2):131–40. doi:10.1360/03ye9014.

Zhang, Y., X. Hu, and X. Wang. 2003. Theoretical analysis of convective heat transfer enhancement of microencapsulated phase change material slurries. *Bubbly Flows: Analysis, Modelling & Calculation* 40 (1):59–66. doi:10.1007/s00231-003-0410-7.

Zhang, Y., Y. Xu, R. Lu, S. Zhang, A. M. Hai, and B. Tang. 2023. Form-stable cold storage phase change materials with durable cold insulation for cold chain logistics of food. *Postharvest Biology and Technology* 203:112409. doi:10.1016/j.postharvbio.2023.112409.

Zhang, Z., G. Shi, S. Wang, X. Fang, and X. Liu. 2013. Thermal energy storage cement mortar containing n-octadecane/expanded graphite composite phase change material. *Renewable Energy* 50:670–75. doi:10.1016/j.renene.2012.08.024.

Zhao, J., J. Zhou, H. Li, and X. Li. 2022. Cuprous oxide modified nanoencapsulated phase change materials fabricated by RAFT miniemulsion polymerization for thermal energy storage and photothermal conversion. *Powder Technology* 399:117189. doi:10.1016/j.powtec.2022.117189.